Composite BNT-BT 0.08 /CoFe 2 O 4 with core-shell nanostructure for piezoelectric and ferromagnetic applications

Composite BNT–$BT_{0.08}$/$CoFe_2O_4$ with core–shell nanostructure for piezoelectric and ferromagnetic applications

M. Cernea[a*], B.S. Vasile[b], I.V. Ciuchi[c,d], V.A. Surdu[b], C. Bartha[a], A. Iuga[a], P. Galizia[c], C. Galassi[c]

[a]National Institute of Materials Physics, P.O. Box MG-7, Bucharest–Magurele, 077125, Romania

[b]University POLITEHNICA of Bucharest, 060042, Romania

[c]National Research Council of Italy – Institute of Science and Technology for Ceramics (CNR–ISTEC), Via Granarolo 64, I–48018 Faenza, Italy

[d]University "Al. I. Cuza", Faculty of Physics, Bv. Carol I, Nr. 11, 700506, Iasi, Romania

ABSTRACT

In this work, we report on the synthesis and characterization of BNT–$BT_{0.08}$/$CoFe_2O_4$ biphasic composite with core–shell structure. This artificial core (BNT–$BT_{0.08}$)/shell ($CoFe_2O_4$) heterostructure was prepared by sol–gel method and the resulting composite was characterized in term of microstructure, dielectric, piezoelectric and magnetic properties. BNT–$BT_{0.08}$/$CoFe_2O_4$ sintered ceramic shows high permittivity ($\varepsilon' \geq 30$) and high dielectric losses ($\tan\delta \geq 10$) in the low frequency range ($\nu \leq 10^4$ Hz), remnant polarization *(Pr)* of ~7.7 $\mu C/cm^2$ and, remanent magnetization (*Mr*) of 24 emu/g at 5 K and of 14 emu/g, at room temperature. The present study reveals that the ferroelectric, piezoelectric and magnetic properties of this new architectured composite depend on the amount of each component and, can be tailored by adjusting their synthesis conditions. BNT–$BT_{0.08}$/$CoFe_2O_4$ core–shell

material investigated in this work provides a novel way to exploit new applications for the multifunctional composite, such as piezoelectric sensor, magnetoelectronic sensors and data storage devices.

KEYWORDS

Lead–free piezoelectric ($(Bi_{0.5}Na_{0.5})_{0.92}Ba_{0.08}TiO_3$); Cobalt ferrite ($CoFe_2O_4$); Sol–gel processes; Composite core–shell.

***Corresponding author**: Marin Cernea

Tel: +40213690170;

Fax: +40213690177;

E-mail address: mcernea@infim.ro; marincernea@yahoo.com

1. Introduction

In the last years, the core-shell nanomaterials have become a research field of great interest due to their potential applications in various fields, like: catalysts, sensors, electronics, optoelectronics and biomedical applications [1,2]. The composite materials consisting of components with distinct properties have also attracted attention due of their potential multifunctional applications [3–5]. New architectures as core–shell composites are already used for some materials, as: bimetallic core–shell nanomaterials [6,7], triple–layered core–shell structure (Au/Co/Fe nanoparticles) [8], $CoFe_2O_4/SiO_2$ nanocomposite core–shell [9], BNT–BTCe/SiO_2 core–shell heterostructure [10], etc. The design of the new types of core–shell nanostructures is an important focus of research and technological development. Here, we report on the core–shell nanostructure of lead-free piezoelectric BNT–$BT_{0.08}$ and ferromagnetic $CoFe_2O_4$ materials. BNT–$BT_{0.08}$ and $CoFe_2O_4$ species can form composites

which should combine their piezoelectric and magnetic properties. These composites belong to the family of magnetoelectric multiferroic materials that display both electric and magnetic order simultaneously [11-15]. The resulting combination of magnetostrictive $CoFe_2O_4$ with piezoelectric BNT–$BT_{0.08}$ presents an artificial multiferroic composite whose electric polarization can be tuned by a magnetic field and whose magnetic properties can be altered by an electric field. An important frontier in nanomaterials synthesis is the growth of crystalline stacked layers on different nanostructures (as grains, layers, wires and tubes) for acquiring controlled chemical and physical properties and new functionalities [16].

In the present study, we describe the processes for the synthesis of high–quality heterojunction BNT–$BT_{0.08}$/$CoFe_2O_4$ core-shell and we investigate its dielectric, piezoelectric and magnetic properties. This new heterostructure was obtained using novel synthesis procedure based on sol–gel chemistry. Different preparation protocols are used here, in order to obtain nano–heterostructure containing BNT–$BT_{0.08}$ and $CoFe_2O_4$ and to improve its structural, ferroelectric and magnetic properties. To the best of our knowledge, there are not reported studies on the composite core–shell BNT–$BT_{0.08}$/$CoFe_2O_4$. There are several publications on each component (BNT–$BT_{0.08}$ and $CoFe_2O_4$), with nanotube [17,18] and thin film [19,20] structure, part of core–shell composites [19] and thin films heterostructures [21]. There are also, few reports on hybrid piezoelectric/ferromagnetic structures, such as: $CoFe_2O_4$/$BaTiO_3$ [22–26], $Pb(Zr_{0.52}Ti_{0.48})O_3$/$NiFe_2O_4$ [27] and $NiFe_2O_4$/$BaTiO_3$ [28] core–shell composites where, the authors studied the influence of ferrite fraction variation on the magnetic properties of the multiferroic core–shell–type nanostructures. Considering that the nanocomposite materials offer a vast design–space of potential material properties depending on the properties of the constituents, we synthesized and studied both electric and magnetic properties of the novel core–shell composite design BNT–$BT_{0.08}$/$CoFe_2O_4$. We compare here our results with those presented in the previous studies [23–29].

2. Experimental

2.1. Materials

Bismuth (III) acetate ($(CH_3COO)_3Bi$, 99.99%), sodium acetate (CH_3COONa, 99.995%), barium acetate ($(CH_3COO)_2Ba$, 99%), titanium (IV) isopropoxide ($Ti\{OCH(CH_3)_2\}_4$) in isopropanol, acetic acid, acetylacetone and formamide were used in order to prepare BNT–$BT_{0.08}$ precursor sol and, cobalt acetate ($Co(CH_3CO_2)_2{\cdot}4H_2O$, 99.995%), iron nitrate ($Fe(NO_3)_3{\cdot}9H_2O$, 99.99%), citric acid ($C_6H_8O_7$, 99%), ethanol, acetic acid and distilled water were used as starting materials to prepare $CoFe_2O_4$ sol precursor. All reagents are provided by Sigma–Aldrich.

2.2. Preparation of BNT–$BT_{0.08}$ and $CoFe_2O_4$ precursor sols

$0.92Bi_{0.5}Na_{0.5}TiO_3$–$0.08BaTiO_3$/$CoFe_2O_4$ (abbreviated as BNT–$BT_{0.08}$/$CoFe_2O_4$) composite core-shell was prepared from BNT–$BT_{0.08}$ and $CoFe_2O_4$ precursor sols. BNT–$BT_{0.08}$ precursor sol was prepared by sol–gel technique using as starting materials sodium acetate, barium acetate, bismuth (III) acetate and titanium (IV) isopropoxide. Acetic acid was used as solvent for the acetates. Sodium acetate and barium acetate are dissolved in acetic acid at 100 °C while bismuth (III) acetate is dissolved in acetic acid at 200 °C. BNT–$BT_{0.08}$ precursor sol was prepared from stoichiometric amount of BNT sol and BT sol. In order to prepare BT precursor sol, the acetic solution of Ba^{2+} was added to titanium (IV) isopropoxide dissolved in isopropanol, at 100 °C, and finally, acetylacetone was added as stabilizer of the resulted sol. The BNT precursor sol is obtained as follows: the Bi^{3+} acetic solution is added to Na^+ solution, then titanium (IV) isopropoxide dissolved in isopropanol and stabilized with acetylacetone was added to the mixture of Bi^{3+} solution and Na^+ solution, at 100 °C. By

adding the sol precursor of BNT to BT sol and stabilized with formamide, a BNT-BT precursor sol was prepared. The sol was further stirred at 80 °C, 2h to homogenize.

$CoFe_2O_4$ sol was prepared from iron nitrate and cobalt acetate. Citric acid was used as chelating agent. Ethanol, acetic acid and water were used here as solvents. The iron nitrate and citric acid were dissolved in ethanol separately, at room temperature. The cobalt acetate was dissolved in ethanol, acetic acid and water. The solutions of iron nitrate and cobalt acetate were first mixed together, and then citric acid solution was added into above solution and stirred at 80 °C to form a cobalt ferrite $CoFe_2O_4$ precursor sol. The molar ratio of Co^{2+}:Fe^{3+}:$C_6H_8O_7$ is 1:2:3.

BNT–$BT_{0.08}$ powder for the core of BNT–$BT_{0.08}$/$CoFe_2O_4$ core–shell composite was prepared from BNT–$BT_{0.08}$ precursor sol, prepared before. The sol was maintained under continuous gently stirring at 75 °C, for 4h, to obtain the gel. After drying the gel at ~100 °C, the resultant powder was calcined at 650 °C, 4 h in air, in order to obtain BNT–$BT_{0.08}$ single–phase powder, as we previously reported [30]. BNT–$BT_{0.08}$ powder de–agglomeration was achieved by dispersion into 2–propanol and sonication for one hour. Then, the sol precursor of $CoFe_2O_4$ was added to the suspension, and kept one day under mechanical stirring in order to obtain a cobalt ferrite layer gel on the BNT–$BT_{0.08}$ particle surface. The resulted coated particles were isolated by centrifugation at 4000 rpm, dried at 100 °C and calcined at 700 °C for 2h, in air. The pellets of BNT–$BT_{0.08}$/$CoFe_2O_4$ obtained by uniaxial pressing were sintered at 1100 °C for 10 min, in air.

2.3. Characterization of material

The crystallographic structure and the composition of the core-shell composites were examined by using a PANalytical Empyrean diffractometer. CuK_α radiation (wavelength 1.5418 Å), e two bounce Ge 220 monochromator and Bragg–Brentano diffraction geometry

were employed. XRD data were acquired at 25 °C with a step-scan interval of 0.02° and a step time of 10s, in the range of 20–80°. The phase content was estimated by Rietveld refinement using a polynomial function for the background fit with flat background, coefficient 1, coefficient 2, coefficient 3 and 1/x, a Pseudo-Voigt profile function and Caglioti function for FWHM approximation. The values of the R factors show a good fitting of the pattern: $R_{profile}$ = 4.6789, $R_{expected}$ = 6.2866, weighted R profile = 6.0263 and χ^2 = 1.9189. The microstructure of the core–shell heterostructures was assessed using a FEI QUANTA INSPECT F scanning electron microscope with field emission gun and a Tecnai™ G^2 F30 S–TWIN transmission electron microscope with a line–resolution of 1 Å, in high resolution transmission electron microscopy (HRTEM) mode. The crystalline structure of the samples was investigated by selected area electron diffraction (SAED). The magnetic hysteresis loops of the core–shell heterostructures were investigated using a Quantum Design MPMS–5S SQUID magnetometer, in the temperature range of 5 K–355 K and an applied magnetic field of up to 70 kOe. The dielectric properties of the samples were studied at room temperature in 100 Hz–1 MHz range of frequency, in the metal–dielectric–metal (MFM) configuration, where the electrodes M consist of silver paste, using a 4194A Impedance/Gain–phase Analyzer. A nominal voltage equal to 0.5 mV was applied. Switching spectroscopy PFM (SS–PFM) measurement of local piezoresponse was performed using an AFM/PFM, Model 5400, from Agilent Technology with a NSC14Ti-Pt probe between -10 V to 10 V.

3. Results and discussion

3.1. Characterization of the structure and microstructure

The result of structural characterization of BNT–$BT_{0.08}$/$CoFe_2O_4$ heterostructured powder, calcined at 700 °C, 2h in air and sintered ceramic at 1100 °C, 10 min, in air, is presented in Fig. 1.

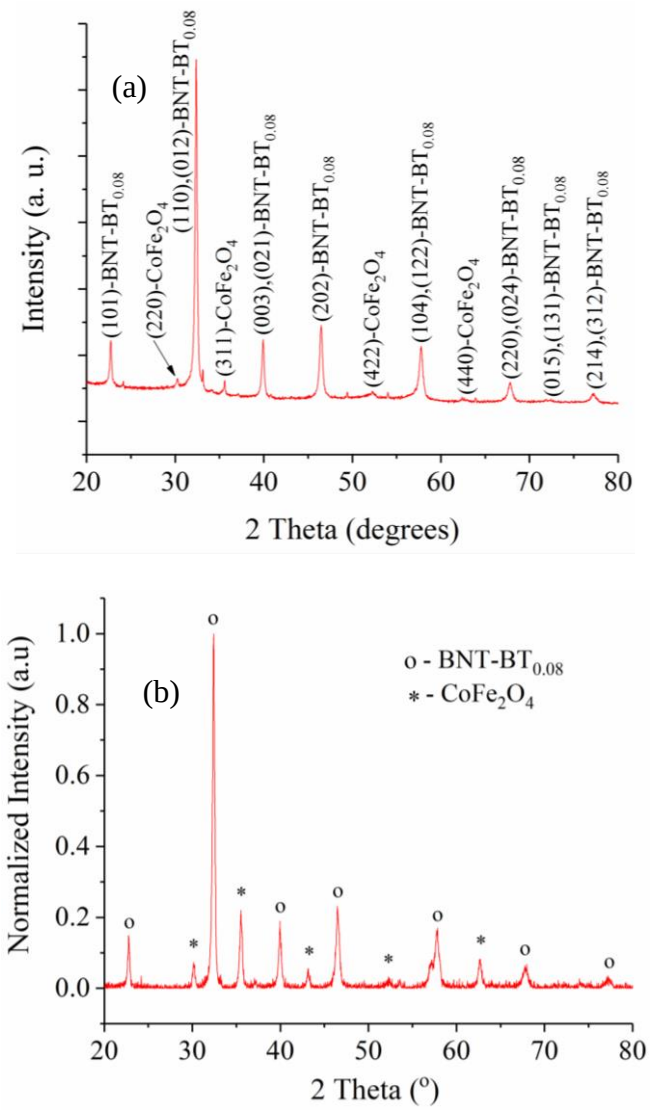

Fig. 1. XRD patterns (CuK$_\alpha$ radiation) of (a) core-shell composite BNT–$BT_{0.08}$/$CoFe_2O_4$ powder calcined at 700 °C, 2h in air and (b) sintered ceramic at 1100 °C, 10 min in air.

According to Fig. 1, the core–shell composite BNT–$BT_{0.08}$/$CoFe_2O_4$ powder has a polycrystalline structure, without any preferred orientation. The X–ray diffraction pattern confirms the presence of structural phases of individual constituents in the composite. The composite, both calcined powder and sintered ceramic, shows only two crystallographic

phases (rhombohedral $Bi_{0.5}Na_{0.5}TiO_3$, space group *R–3m*, *Pattern*: 04–015–0482 [31]) corresponding to the core and (cubic $CoFe_2O_4$, space group *Fd–3m*, *Pattern*: 04–005–7078 [32]) corresponding to the shell layer. For BNT–$BT_{0.08}$/$CoFe_2O_4$ core–shell powder, the phase content, estimated by Rietveld refinement, is 95.9 wt. % BNT–$BT_{0.08}$ and 4.1 wt.% $CoFe_2O_4$.

BNT–$BT_{0.08}$ powder used as core in BNT–$BT_{0.08}$/$CoFe_2O_4$ composite core–shell shows a microstructure consisting of non–uniform (both in shape and size) grains with an average grain size of 75 nm (Fig. 2a).

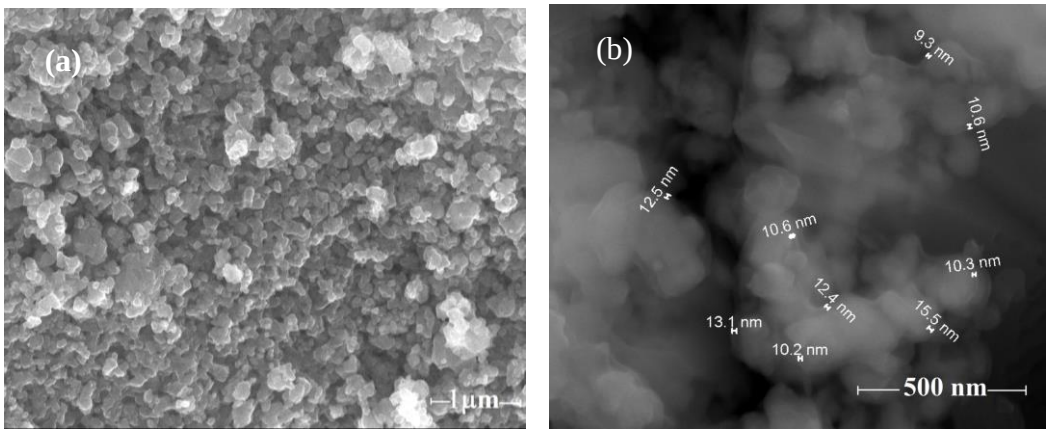

Fig. 2. SEM image of core BNT–$BT_{0.08}$ powder calcined at 650 °C, 4 h in air (a) and SEM image of BNT–$BT_{0.08}$/$CoFe_2O_4$ core–shell powder dried at 100 °C (b).

The core–shell composite BNT–$BT_{0.08}$/$CoFe_2O_4$ powder, dried at 100 °C, presents grains of 90–95 nm average diameter and a nanoshell with an estimated thickness of 15–20 nm (Fig. 2b and Fig. 3a). The phase contrast TEM image Fig. 3a and detail Fig. 3b provide views of nanoparticles of the calcined BNT–$BT_{0.08}$/$CoFe_2O_4$ core/shell nanostructure.

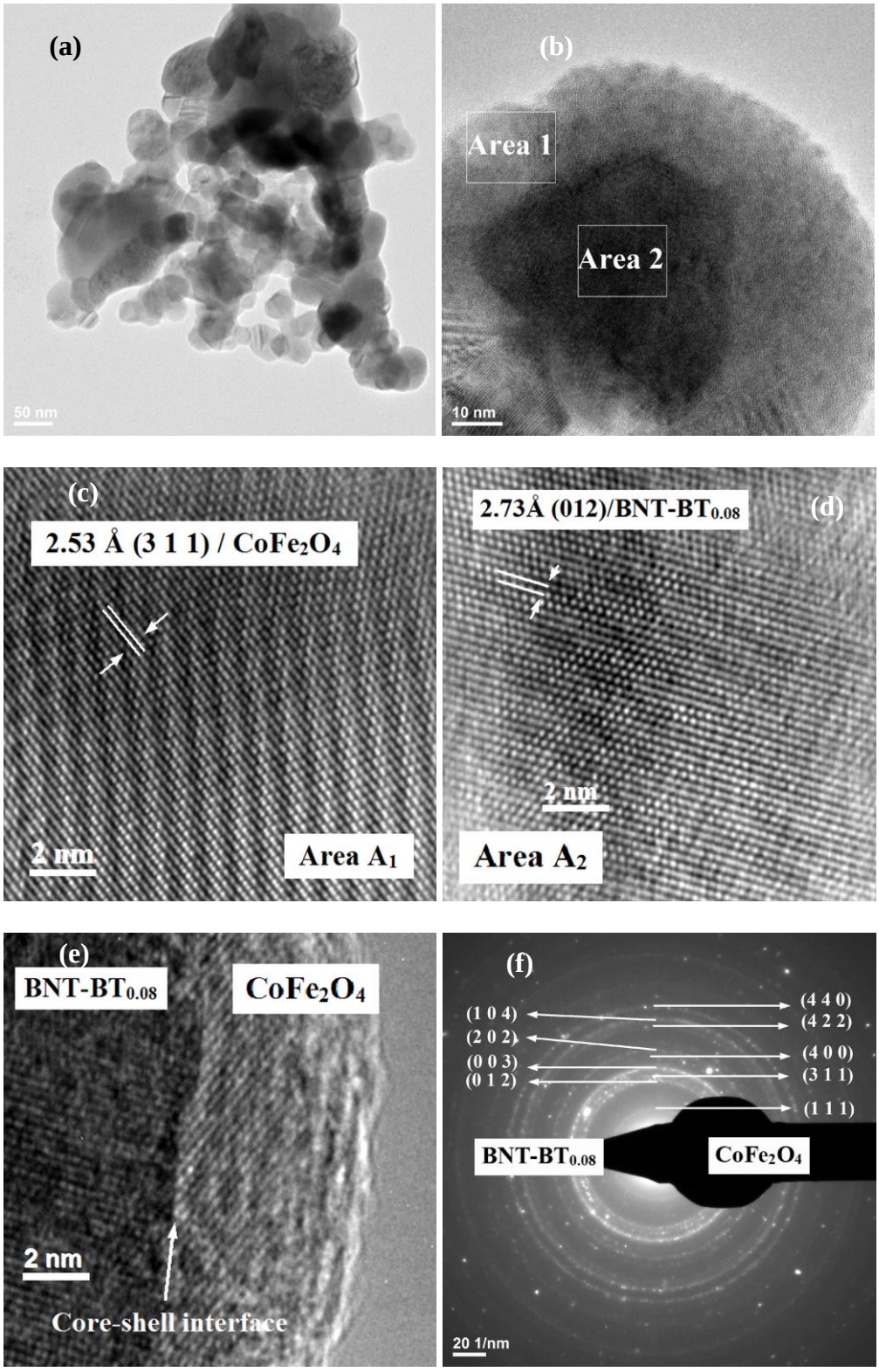

Fig. 3. (a) BF–TEM and (b) detail images of the core-shell BNT–$BT_{0.08}$/$CoFe_2O_4$ calcined powder at 700 °C for 2h, in air. (c)-(e) HR–TEM of Area 1, Area 2 and between the two Areas (phases), respectively. (f) Corresponding SAED pattern of the calcined powder.

Typical lattice resolved HRTEM images of BNT–$BT_{0.08}$/$CoFe_2O_4$ core–shell powder (Area A_1 for $CoFe_2O_4$ shell and Area A_2 for BNT–$BT_{0.08}$ core) indicate that the powder did not have an anisotropic growth. The BNT–$BT_{0.08}$/$CoFe_2O_4$ nanocrystals have different orientations. Both HRTEM and circular distinct ring patterns corresponding to the different lattice planes observed in the SAED pattern confirm the core–shell heterostructure with rhombohedral BNT–$BT_{0.08}$ and cubic $CoFe_2O_4$ phases. HRTEM micrograph of core - shell interface (Fig. 3e) shows clearly the existence of an interface between grain core and layer shell.

The morphology of BNT–$BT_{0.08}$/$CoFe_2O_4$ sintered ceramic and the elements distribution were investigated through SEM images and presented in Fig. 4.

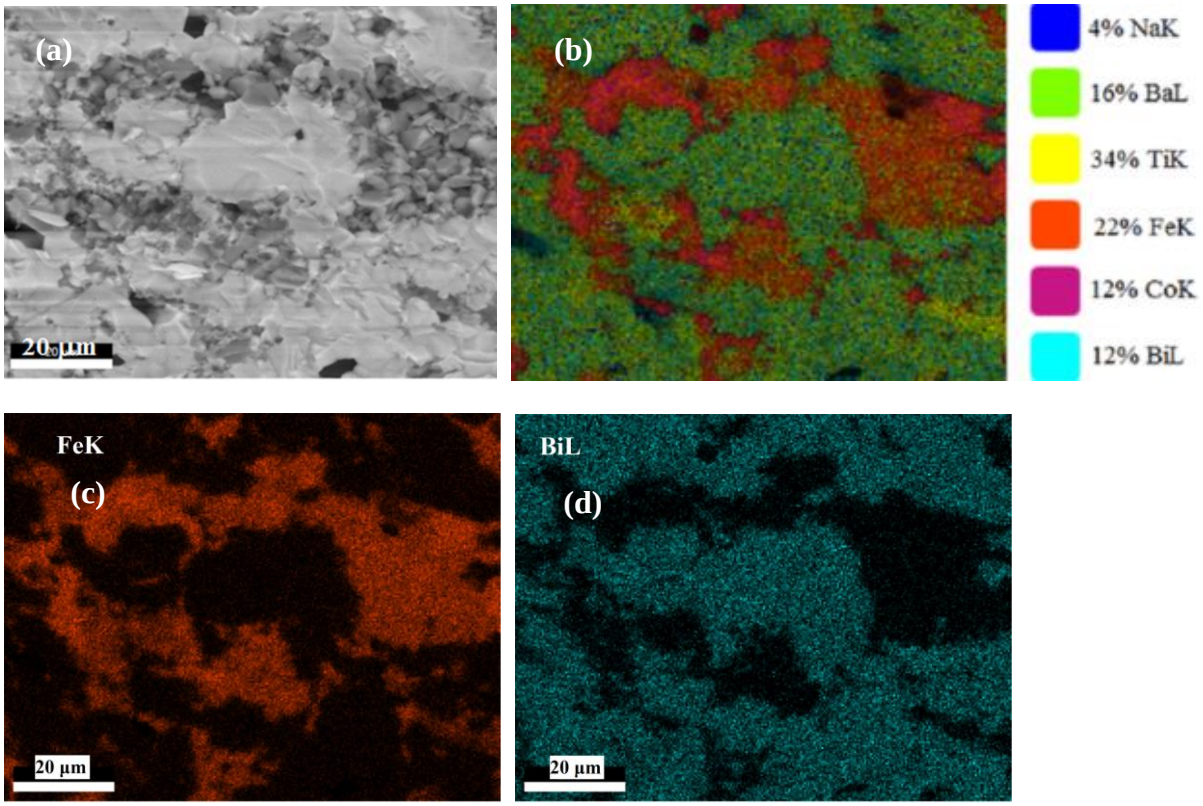

Fig. 4. (a) SEM micrograph of fracture surface of sintered ceramic BNT–$BT_{0.08}$/$CoFe_2O_4$ at 1100 °C, 10 min in air and, (b–d) corresponding chemical compositional mapping.

The SEM micrograph of the fresh fracture surface of sintered pellets indicated areas with grains of various sizes, having the composition of $CoFe_2O_4$, separated by areas with continuous morphology of BNT–$BT_{0.08}$ phase. Backscattered electrons (BSE) are used to detect contrast between areas with different chemical compositions (Fig. 4a). The area-mapping of EDX (Fig. 4b–d) indicates that the elements Na, Ba, Ti, Fe, Co and Bi are uniformly distributed on areas of fracture surface of ceramic, corresponding to the two phases $CoFe_2O_4$ and BNT–$BT_{0.08}$. The separation of the two phases in different regions is evident in the SEM images of Fig. 4 a–d. BNT–$BT_{0.08}$/$CoFe_2O_4$ sintered samples show an apparent density of 5.535 g/cm^3. Apparent densities of the sintered pellets were measured by Archimedes method (in distilled water) using a density balance. Considering the phases composition data from XRD analysis, we calculated a theoretical density for BNT–$BT_{0.08}$/$CoFe_2O_4$ core–shell composite of 5.96 g/cm^3. The relative density ρ_{ap}/ρ_{theor} = 93 % indicates close packed grain structure due to an advanced degree of sintering.

3.2. Dielectric characterization

The complex dielectric properties and conductivity behavior of the core-shell BNT–$BT_{0.08}$/$CoFe_2O_4$ sintered pellets at 1100 °C, 10 min, in air were investigated at room temperature and frequency between 1 Hz and 1 MHz.

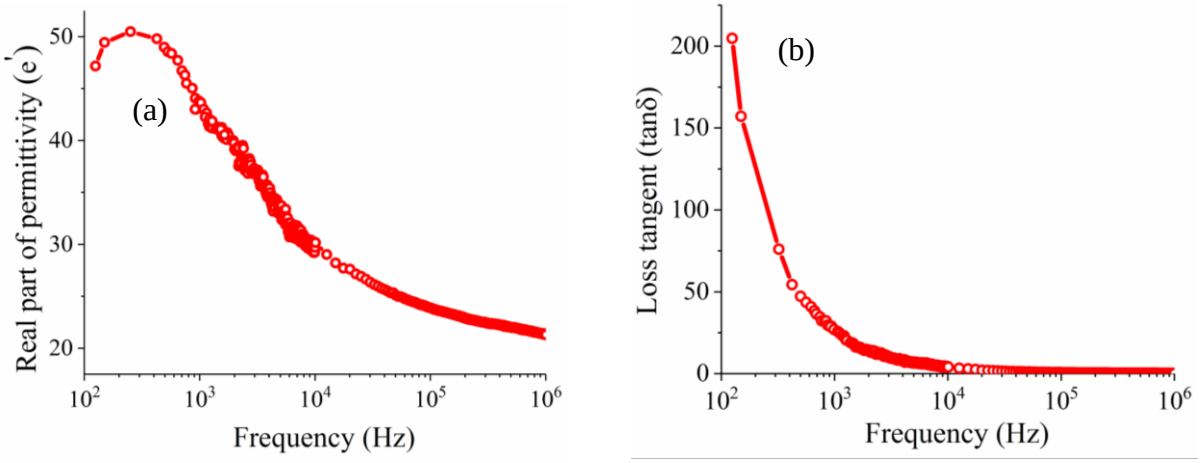

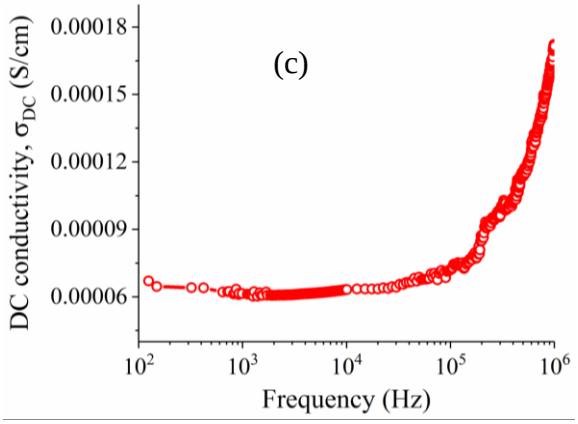

Fig. 5. Frequency dependence of (a) real part of the permittivity, (b) loss tangent, and (c) of the AC conductivity for BNT–$BT_{0.08}$/$CoFe_2O_4$ sintered composite core-shell.

Due to the coexistence of semi conductive $CoFe_2O_4$ [33] and resistive BNT–$BT_{0.08}$ [34] phases in the studied pellets, the electrical properties of BNT–$BT_{0.08}$/$CoFe_2O_4$ composite core–shell ceramic are complicated, depending on the physical microstructure (morphology) and the material properties of the two phases in a complex way [35]. The frequency dependence of the real part of dielectric constant (ε'), and loss tangent (*tan* δ) of BNT–$BT_{0.08}$/$CoFe_2O_4$ multiferroic composite ceramic, measured at room temperature, in the frequency range 100 Hz–1 MHz, are shown in Fig. 5a,b. It is clear from these figures that the dielectric constant and *tan* δ are strongly dependent on the frequency. The dielectric constant (ε') and *tan* δ initially showed a sharp decrease with increase in frequency up to 1 kHz and then decreased slowly and become almost constant up to 1MHz, indicating a typical Maxwell–Wagner dielectric dispersion. This Maxwell–Wagner type relaxation may be associated with the existence of significant, but inhomogeneous electrical conduction in the material originated from $CoFe_2O_4$ phase [33]. Similar with other reports on different core-shell ceramics composites [36,10], the high values of permittivity ($\varepsilon' \geq 30$) together with high dielectric losses (tan $\delta \geq 10$) for BNT–$BT_{0.08}$/$CoFe_2O_4$ core–shell nanostructure in the low

frequency range ($\nu \leq 10^4$ Hz) may be also related to interfacial polarization coming from grain boundaries and surface polarization. The dielectric losses are minimized in the highest frequency range ($\nu \geq 10$ kHz) showing tan $\delta \leq 3.3$ for BNT–$BT_{0.08}$/$CoFe_2O_4$ sample. In addition, following a similar approach as we did in a previous paper [33], we have investigated the variation of conductivity, complex dielectric modulus and complex impedance spectrum as a function of frequency. The results are shown in Fig. 5c and Fig. 6a-c.

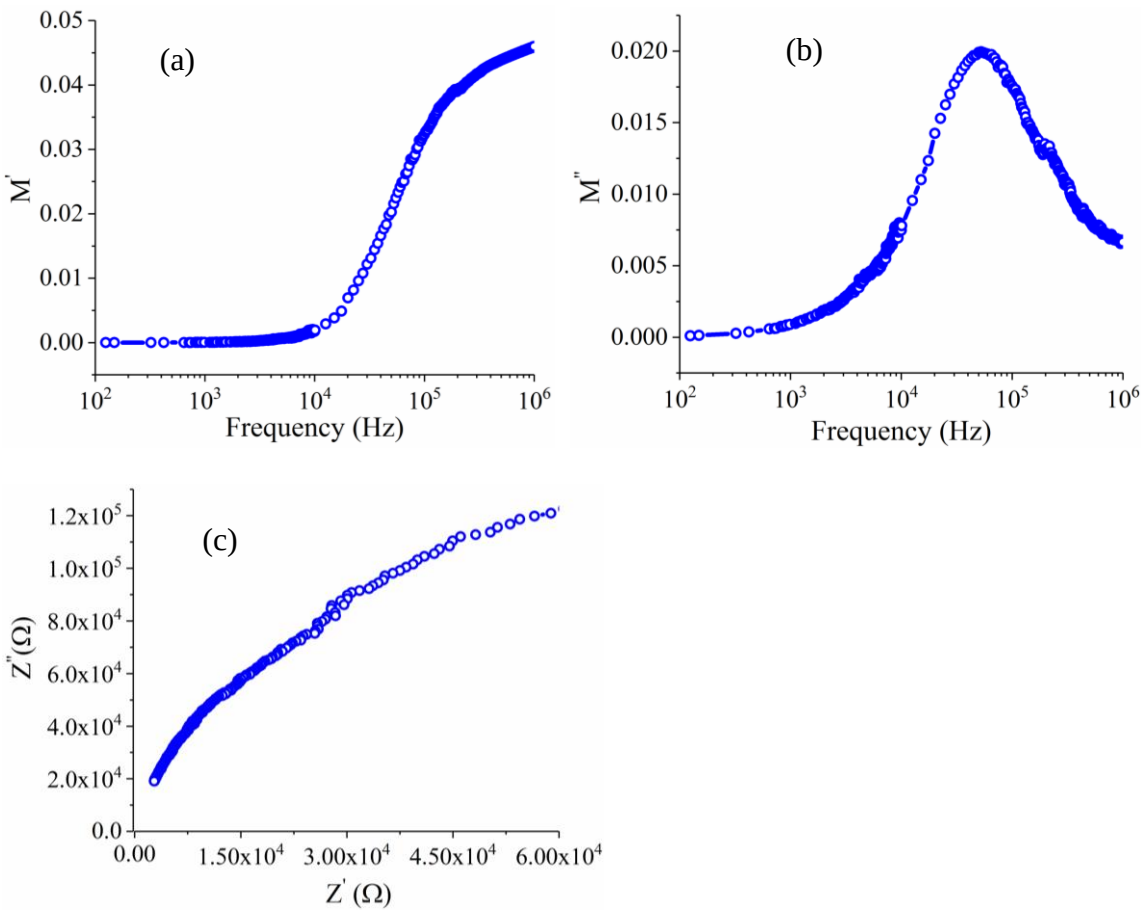

Fig. 6. (a) Real (M′) and (b) imaginary (M′′) parts of electric modulus as a function of frequency; (c) Nyquist plot obtained at room temperature for BNT–$BT_{0.08}$/$CoFe_2O_4$ sintered composite core-shell.

As suggested by the increase of conductivity and real part of dielectric modulus in the high frequency region, the presence of the maximum in the imaginary part of dielectric modulus, the asymmetric Nyquist plot, the sample shows ionic conduction. The maximum in the imaginary part of dielectric modulus was previously observed in $CoFe_2O_4$ at much higher frequency (i.e.: $\nu \geq 7 \cdot 10^5$ Hz) [33]. This maximum separates the frequency range in which charge carriers are mobile on long distances from frequency range on which those are mobile on short distances [37–39]. It is worth noting that, in respect to the cited article [40], in our samples it is shifted at lower frequency. In addition, the dielectric losses show values much lower respect to $CoFe_2O_4$ [33] phase which means that combining BNT–$BT_{0.008}$ with $CoFe_2O_3$ in a core–shell structure improves the dielectric performance of $CoFe_2O_3$ phase.

3.3. Ferroelectric properties

For polarization measurements of BNT–$BT_{0.08}$/$CoFe_2O_4$ sintered composite core–shell, the PUND (positive–up, negative–down) method has been used (Fig. 7). This procedure eliminates of all the losses except those proper to the remanent switch processes.

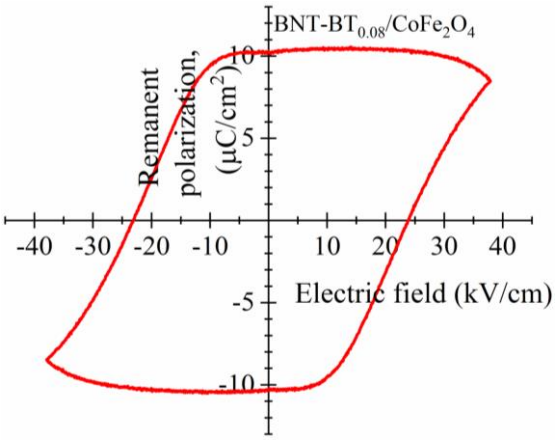

Fig. 7. Polarization hysteresis loop obtained by PUND method at room temperature for BNT–$BT_{0.08}$/$CoFe_2O_4$ sintered ceramic sample.

PUND like measurement were performed over the whole range of voltages suitable for the sample, from –75.5 kV/cm to 75.5 kV/cm (Fig. 7). The polarization loop recorded for BNT–$BT_{0.08}$/$CoFe_2O_4$ sample at room temperature, has a normal shape, indicating low remanent switch losses (Fig. 7). The remanent polarization loop of BNT–$BT_{0.08}$/$CoFe_2O_4$ sintered core–shell heterostructure is well saturated and the remanent polarization value is ~7.7 μC/cm^2 indicating that the sample show ferroelectric properties.

3.4. Piezoelectric characterization

For the ceramics pellets samples of composite core–shell BNT–$BT_{0.08}$/$CoFe_2O_4$ it not was possible to reach saturation during the electric poling process due to the ferrite phase with low resistivity and therefore, the piezoelectric coefficient measurement was not performed. In this case, the electromechanical properties of BNT–$BT_{0.08}$/$CoFe_2O_4$ sintered ceramic composite were investigated by piezoelectric force microscopy, as shown in Fig. 8. The measurements of local hysteresis loops of material are quite rarely done on ceramics because of the unknown orientation of a particular grain and, the existence of the grain boundaries where mechanical stresses, uncompensated charges, and defects are concentrated. The phase signal can be linked to the spontaneous polarization orientation, while PFM amplitude is a function of local effective piezoelectric coefficient [36].

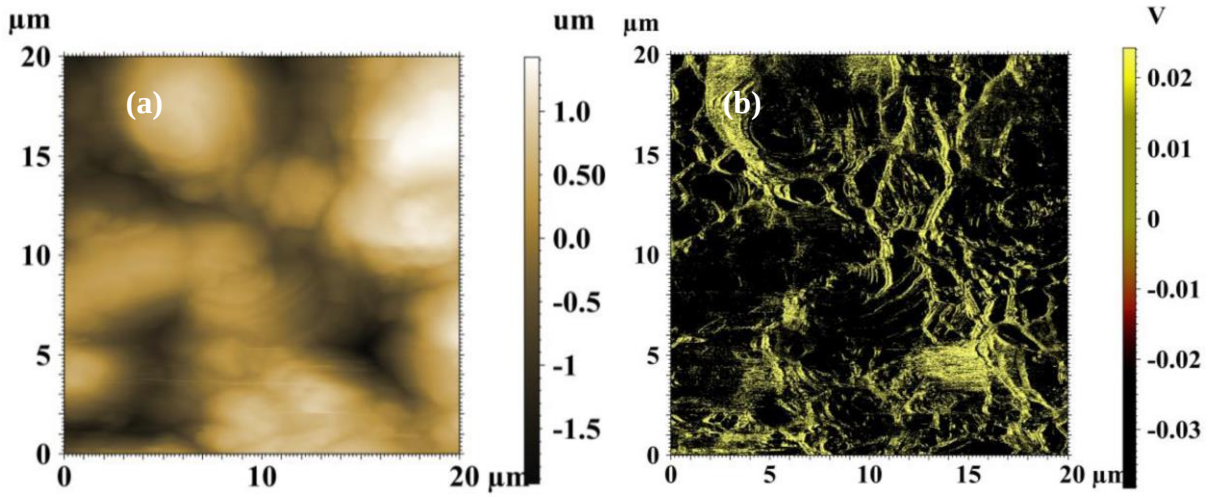

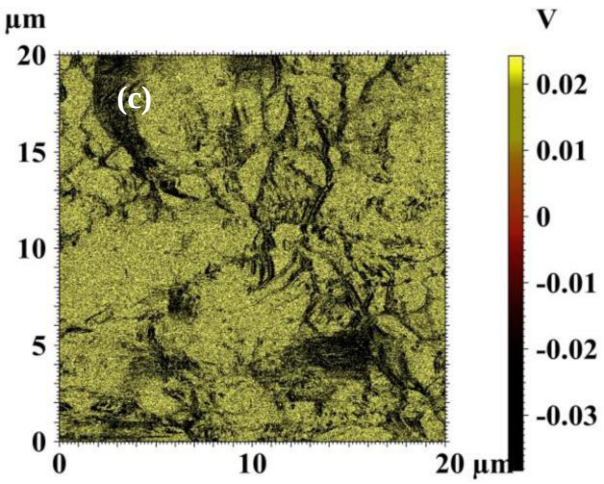

Fig. 8. Piezoelectric characterization and polarization hysteresis measurements of the BNT–$BT_{0.08}$/$CoFe_2O_4$ core–shell sintered ceramic. AFM contact mode topography (a); simultaneously acquired maps of amplitude (b) and phase (c) of piezoresponse.

Ferroelectric domains with opposite piezoresponse, i.e., bright and dark colors in PFM, which correspond to ferroelectric domains, are evident in PFM phase mapping of BNT–$BT_{0.08}$/$CoFe_2O_4$ ceramic sample. In the phase images, a not uniform polarization could be observed for the composite core–shell and this result can be understood by the two–phase (here $CoFe_2O_4$ and BNT–$BT_{0.08}$ phases) model, applicable to the multiferroic heterostructures [22,41–43]. After applying a reverse voltage, the polarization could be well switched into the reverse direction, as indicated by the change of phase contrast in the polarized area (Fig. 8c). Polarization switching was further confirmed by a piezoelectric hysteresis loop, which is rather square (Fig. 7). The coexistence of the regions demonstrating a distinct PFM contrast with the areas showing a zero piezoresponse corresponding to $CoFe_2O_4$ grains was also observed in this composite core–shell. The piezoresponse contrast distribution corresponding to the domain structure varies significantly among the grains, as expected for a non–oriented ceramics. In BNT–$BT_{0.08}$/$CoFe_2O_4$ core–shell heterostructure, the ferroelectric domains form

long chains (a labyrinth–shaped pattern) and their high amount is in good agreement with polarization hysteresis measurements (Fig. 7). So, the existence of ferroelectric domains confirms the local piezoelectricity of this core–shell composite.

3.5. Magnetic characterization

Magnetic hysteresis loops for the core–shell powders coming from crushed sintered pellets, were performed at two different temperatures (5 K and 295 K). Figure 9a,b shows the magnetization versus magnetic field (*M–H*) loops of BNT–$BT_{0.08}$/$CoFe_2O_4$ powder core-shell obtained by applying field up to 70 kOe at 5 K and 295 K, respectively.

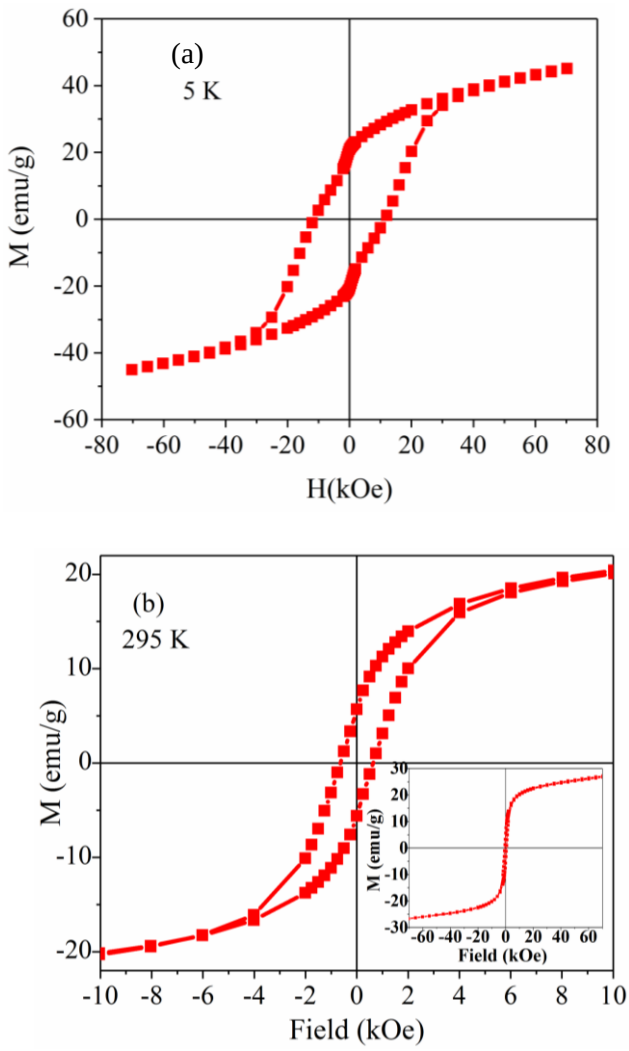

Fig. 9. Magnetic hysteresis curves recorded at 5 K (a) and 295 K (inset of (b)) for the core/shell hetero–nanostructure BNT-$BT_{0.08}$/$CoFe_2O_4$ powder; (b) shows the magnified part of the hysteresis loop in the low–field range, of the composite.

The core–shell composite BNT–$BT_{0.08}$/$CoFe_2O_4$ exhibits at low temperature (5 K) and at room temperature (295 K), typical magnetic hysteresis loops, as well as remnant magnetization indicating the presence of an ordered magnetic structure. The values of magnetic parameters corresponding to the BNT–$BT_{0.08}$/$CoFe_2O_4$ composite are listed in Table 1.

Table 1

Magnetic parameters of the core–shell BNT–$BT_{0.08}$/$CoFe_2O_4$ powder measured at 5 K and 295 K (results from the literature are reported as well, for comparison).

Core-shell powders samples	Temp. (K)	M_r (emu/g)	H_c (kOe)
BNT–$BT_{0.08}$/$CoFe_2O_4$;	5	24	11.9
(95.4% BNT–$BT_{0.08}$/4.6% $CoFe_2O_4$)	295	14	2.3
$CoFe_2O_4$ powder [33]	5	-	-
	300	27.2	6.84
$CoFe_2O_4$ bulk [33]	5	74.2	20.09
	300	21.2	1.41
$CoFe_2O_4$/$BaTiO_3$ [26]	RT	9.96	2.2
$CoFe_2O_4$/$BaTiO_3$ [27]	RT	9.52	0.87
$Pb(Zr_{0.52}Ti_{0.48})O_3$/$NiFe_2O_4$ [28]	RT	-	0.216
$NiFe_2O_4$/$BaTiO_3$ [29]	RT	-	~0.050

where: RT is room temperature and, phases contents (wt.%) were obtained by Rietveld refinement.

The magnetization curves does not reach the saturation, therefore, just the value of remanent magnetization (*Mr*) and coercivity field (*Hc*) for the nanocomposite core-shell BNT–$BT_{0.08}$/$CoFe_2O_4$ are discussed. The values of magnetic parameters of the core-shell BNT–$BT_{0.08}$/$CoFe_2O_4$ powder are lower than those of the $CoFe_2O_4$ nanoparticles and bulk [33], as can be seen in Table 1. For $CoFe_2O_4$, a decrease in magnetization from bulk values to powder values is typical of magnetic nanoparticles and can result from several factors usually collectively referred to as size or surface effects [24]. The most important parameter that contributes to the ferromagnetic behavior of this composite is the amount of magnetic phase $CoFe_2O_4$. Thus, BNT–$BT_{0.08}$/$CoFe_2O_4$ core–shell nanocomposite shows lower *Hc* and *Mr* values than $CoFe_2O_4$ powder and bulk due to lower content of $CoFe_2O_4$ in the shell with thickness of 15–20 nm. Small magnetic shell thickness will provide high resistivity in the sintered composite and reduce the additional misfit strain caused by different striction of the adjacent phases, as reported Islam et al. [28] for (1–x)$Pb(Zr_{0.52}Ti_{0.48})O_3$–x$Ni_{0.8}Zn_{0.2}Fe_2O_4$. Also, there is the possibility to have a crystallographic distortion for the cobalt ferrite of the shell, leading to some inversions or cation redistributions in the spinel structure which could also contribute to the decrease of the magnetization in BNT–$BT_{0.08}$/$CoFe_2O_4$ composite [44,45]. It is known that the changes in the magnetic properties can be related to different grain sizes, anti–phase boundaries, and interface hybridization effects [44,46,47]. No saturation is reached and, this behavior is related to the relative increase of the surface as particles size decreased and to the increases role of the disordered magnetic structure of the surface nanoparticle. The shape of the hysteresis obtained at 5 K for the core-shell composite confirms the existence of a pronounced anisotropy of the magnetic component which inhibits

the alignment of the magnetic moments in applied magnetic field and is due to surface effects.

Note that the form of the hysteresis recorded at 5 K suggests a superposition of two different hysteresis. These two hysteresis can be correlated with the existence of two distinct magnetic phases not coupled by exchange interactions. Given that $(Hc)_{left}$ = -12.04756 kOe and $(Hc)_{right}$ = 12.04815 kOe (Fig. 9a), result that there are no sub-lattices with non-compensating spins. Furthermore, the shoulder on the hysteresis (at M = 18.56 emu/g) indicates distinct non-coupled magnetic phases. Theoretical calculation made for various perovskite materials, such as $Bi_{0.5}Na_{0.5}TiO_3$, $PbTiO_3$, $BaTiO_3$, or $SrTiO_3$ have predicted the ferromagnetism of these materials, derived from self–defects such as Ti or O vacancies [48–50]. In addition, the experimental results also demonstrated that the magnetic nanosized oxides are ferromagnetic, due to the exchange interactions between localized electron spin moments and oxygen vacancies at the surface of the nanoparticles [51,52]. Therefore, the core BNT–$BT_{0.08}$ is a material with diluted magnetic properties compared to the shell $CoFe_2O_4$ which is a hard magnetic material; so, the very large coercive field at low temperature (5 K) that indicates a high anisotropy is due to the cobalt ferrite. The anisotropy at high temperature (room temperature) is lower than that at 5 K, which is shown by the coercive field.

If we compare the magnetic properties of BNT–$BT_{0.08}$/ $CoFe_2O_4$ multiferroic core–shell nanocomposite with reported values for $CoFe_2O_4$/$BaTiO_3$ [26,27] and $NiFe_2O_4$/$BaTiO_3$ [29], our composite shows higher Mr and Hc values than those reported [26-29] (Table 2). BNT–$BT_{0.08}$/$CoFe_2O_4$ core–shell composite shows higher Hc than $Pb(Zr_{0.52}Ti_{0.48})O_3$/$NiFe_2O_4$ [28].

Because the remanent magnetization is less than half of the maximum magnetization (70 kOe), it can be concluded that there are no inter–particle interactions [53]. Therefore, there are intra–particle and interfaces interactions which influence the overall magnetism of a

ferroelectric/ferromagnetic system [54,23–29]. According to these reports, our results suggest that in the composite core–shell BNT–$BT_{0.08}/CoFe_2O_4$, the intra–particle magnetic interactions can influence the spin structure of nanoparticles and the magnetic properties of the core–shell composite.

4. Conclusions

In summary, we have prepared core shell composite BNT–$BT_{0.08}/CoFe_2O_4$ powder and ceramic, using the sol–gel chemistry. XRD, SEM, HRTEM and SAED investigation demonstrated the core–shell structure of this composite. The ordering of dopant and the formation of separate phases in these materials has been highlighted by scanning electron microscopy. This composite shown rhombohedral $Bi_{0.5}Na_{0.5}TiO_3$ crystallographic phase (95.9 wt. %) in the core and, cubic $CoFe_2O_4$ phase (4.1 wt.%) in the shell layer, as resulted from XRD investigations. High values of permittivity ($\varepsilon' \geq 30$) together with high dielectric losses ($\tan \delta \geq 10$) were obtained for BNT–$BT_{0.08}/CoFe_2O_4$ core–shell nanostructure in the low frequency range ($\nu \leq 10^4$ Hz). The remanent polarization value of BNT–$BT_{0.08}/CoFe_2O_4$ sintered core–shell heterostructure is ~7.7 μC/cm^2 indicating that the sample show ferroelectric properties. The values of magnetic parameters of the core–shell BNT–$BT_{0.08}/CoFe_2O_4$ powder are *Mr* = 14 emu/g and *Hc* = 2.3 kOe, at room temperature. This composite shows ferroelectric domains that confirm its local piezoelectricity. Our investigations showed that the core grain size and layer shell thickness influence the ratio of electric and ferromagnetic properties for this core–shell composite. These results on BNT–$BT_{0.08}/CoFe_2O_4$ core–shell nanostructures can stimulate the development of submicro- and nano-scale devices like nanoscale capacitors, piezoelectric nanosensor and magnetoelectronic devices.

Acknowledgements

The authors would like to thank Dr. L. Diamandescu for helpful comments on the XRD analyses. The SEM analyses on the samples were possible due to EU–funding grant POSCCE–A2–O2.2.1–2013–1/Priority direction 2, Project No.638/12.03.2014, cod SMIS–CSNR 48652.

References

[1] C.T. Campbell, S.C. Parker, D.E. Starr, The effect of size–dependent nanoparticle energetics on catalyst sintering, Science 298 (2002) 811–814.

[2] H.N. Tsao, D. Cho, J.W. Andreasenetal, The influence of morphology on high–performance polymer field–effect transistors, Adv. Mater. 21 (2009) 209–2012.

[3] L. Zhang, J. Zhai, W. Mo, X. Yao, The dielectric and leakage current behavior of $CoFe_2O_4$–$BaTiO_3$ composite films prepared by combining method of sol–gel and electrophoretic deposition, Solid State Sci. 12 (2010) 509–514.

[4] S.Y. Tan, S.R. Shannigrahi, S.H. Tan, F.E.H. Tay, Synthesis and characterization of composite $MgFe_2O_4$–$BaTiO_3$ multiferroic system, J. Appl. Phys. 103 (2008) 094105–4.

[5] J.P. Zhou, Z.C. Qiu, P. Liu, Electric and magnetic properties of $Pb(Zr_{0.52}Ti_{0.48})O_3$–$CoFe_2O_4$ particle composite thin film on the $SrTiO_3$ substrate, Mater. Res. Bull. 43 (2008) 3514–3520.

[6] C. Wang, D. van der Vliet, K.L. More, N.J. Zaluzec, S. Peng, S. Sun, H. Daimon, G. Wang, J. Greeley, J. Pearson, et al., Multimetallic Au/$FePt_3$ nanoparticles as highly durable electrocatalyst, Nano Lett. 11 (2011) 919–926.

[7] X. Liu, D. Wang, Y. Li, Synthesis and catalytic properties of bimetallic nanomaterials with various architectures (Review), Nano Today 7 (2012) 448–466.

[8] K. Aranishi, H.L. Jiang, T. Akita, M. Haruta, Q. Xu, One-step synthesis of magnetically recyclable Au/Co/Fe triple-layered core-shell nanoparticles as highly efficient catalysts for the hydrolytic dehydrogenation of ammonia borane, Nano Res. 4 (2011) 1233–1241.

[9] Y. Xu, Y. Ma, S. Xu, G. Zheng, Z. Dai, Diluted and undiluted monodispersed $CoFe_2O_4$ nanoparticles: the effects of post-annealing on magnetic properties, J. Mater. Sci. 50 (2015) 4486−4494.

[10] M. Cernea, B.S. Vasile, I.V. Ciuchi, A. Iuga, E. Alexandrescu, J. Pintea, C. Galassi, Synthesis, structural and electrical properties of BNT–BTCe@SiO_2 core–shell heterostructure, Sci. Adv. Mater. 7 (2015) 2297–2305.

[11] N.A. Spaldin, M. Fiebig, The Renaissance of Magnetoelectric Multiferroics, Science 309 (2005) 391–392.

[12] W. Eerenstein, N.D. Mathur, J.F. Scott, Multiferroic and Magnetoelectric Materials, Nature 442 (2007) 59–65.

[13] A. Ahlawat, S. Satapathy, M.M. Shirolkar, J. Li, A.A. Khan, P. Deshmukh, H. Wang, R.J. Choudhary, A.K. Karnal, Tunable Magnetoelectric Nonvolatile Memory Devices Based on $SmFeO_3$/P(VDF-TrFE) Nanocomposite Films, ACS Appl. Nano Mater. 1 (2018) 3196-3203.

[14] A. Ahlawat, S. Satapathy, P. Deshmukh, M.M. Shirolkar, A.K. Sinha, A.K. Karnal, Electric field poling induced self-biased converse magnetoelectric response in PMN-PT/$NiFe_2O_4$ nanocomposites, Appl. Phys. Lett. 111 (2017) 262902-5.

[15] M.M. Shirolkar, R. Das, T. Maity, P. Poddar, S.K. Kulkarni, Observation of Enhanced Dielectric Coupling and Room-Temperature Ferromagnetism in Chemically Synthesized $BiFeO_3$@SiO_2 Core–Shell Particles, J. Phys. Chem. C, 116 (2012) 19503-19511.

[16] B. Mukherjee, A. Peterson, V. Subramanian, 1D CdS/PbS heterostructured nanowire synthesis using cation exchange, Chem Commun. 48 (2012) 2415–2417.

[17] M. Cernea, L. Trupina, B.S. Vasile, R. Trusca, C. Chirila, Nanotubes of piezoelectric BNT-$BT_{0.08}$ obtained from sol-gel precursor, J. Nanopart. Res. 15 (2013) 1787–1795.

[18] Y. Xu, J. Wei, J. Yao, J. Fu, D. Xue, Synthesis of $CoFe_2O_4$ nanotube arrays through an improved sol–gel template approach, Mater. Lett. 62 (2008) 1403–1405.

[19] M. Cernea, L. Trupina, C. Dragoi, A.C. Galca, L. Trinca, Structural, optical, and electric properties of BNT–$BT_{0.08}$ thin films processed by sol-gel technique, J. Mater. Sci. 47 (2012) 6966–6971.

[20] M. Kumari, A. Singh, A. Gupta, C. Prakash, R. Chatterjee, Self–biased large magnetoelectric coupling in co–sintered $Na_{0.5}Bi_{0.5}TiO_3$ based piezoelectric and $CoFe_2O_4$ based magnetostrictive bilayered composite, J. Appl. Phys. 116 (2014) 244101 (1–5).

[21] J.G. Wan, X.W. Wang, Y.J. Wu, M. Zeng, Y. Wang, H. Jiang, W.Q. Zhou, G.H. Wang, J.M. Liu, Magnetoelectric $CoFe_2O_4$–$Pb(Zr,Ti)O_3$ composite thin films derived by a sol-gel process, Appl. Phys. Lett. 86 (2005) 122501 (1–3).

[22] X. Gao, B.J. Rodriguez, L. Liu, B. Birajdar, D. Pantel, M. Ziese, M. Alexe, D. Hesse, Microstructure and properties of well ordered multiferroic $Pb(Zr,Ti)O_3$/$CoFe_2O_4$ nanocomposites, ACS Nano 4 (2010) 1099–1107.

[23] M. Etie, C. Schmitz-Antoniak, S. Salamon, H. Trivedi, Y. Gao, A. Nazrabi, J. Landers, D. Gautam, M. Winterer, D. Schmitz, H. Wende, V.V. Shvartsman, D.C. Lupascu, Magnetoelectric coupling on multiferroic cobalt ferrite–barium titanate ceramic composites with different connectivity schemes, Acta Materialia 90 (2015) 1–9.

[24] V. Corral–Flores, D. Bueno–Baques, R.F. Ziolo, Synthesis and characterization of novel $CoFe_2O_4$–$BaTiO_3$ multiferroic core–shell–type nanostructures, Acta Materialia 58 (2010) 764–769.

[25] V.V. Shvartsman, F. Alawneh, P. Borisov, D. Kozodaev, D.C. Lupascu, Converse magnetoelectric effect in $CoFe_2O_4$–$BaTiO_3$ composites with a core–shell structure, Smart Mater. Struct. 20 (2011) 075006 (1–6).

[26] S. Betal, M. Dutta, L.F. Cotica, A. Bhalla, R. Guo, $BaTiO_3$ Coated $CoFe_2O_4$–Core-Shell Magnetoelectric Nanoparticles (CSMEN) Characterization, Integrated Ferroelectrics, 166 (2015) 225–231.

[27] P.N. Oliveira, D.M. Silva, G.S. Dias, I.A. Santos, L.F. Cotica, Synthesis and physical property measurements of $CoFe_2O_4$:$BaTiO_3$ core–shell composite nanoparticles, Ferroelectrics 499 (2016) 76–82.

[28] R.A. Islam, V. Bedekar, N. Poudyal, J.P. Liu, S. Priya, Effect of piezoelectric grain size on magnetoelectric coefficient of $Pb(Zr_{0.52}Ti_{0.48})O_3$–$Ni_{0.8}Zn_{0.2}Fe_2O_4$ particulate composites, J. Appl. Phys. 104 (2008) 104111 (1–4).

[29] J.P. Zhou, L. Lv, Q. Liu, Y.X. Zhang, P. Liu, Hydrothermal synthesis and properties of $NiFe_2O_4$@$BaTiO_3$ composites with well–matched interface, Sci. Technol. Adv. Mater. 13 (2012) 045001 (1–12).

[30] M. Cernea, E. Andronescu, R. Radu, F. Fochi, C. Galassi, Sol–gel synthesis and characterization of $BaTiO_3$ doped–$(Bi_{1/2}Na_{1/2})TiO_3$ piezoelectric ceramics, J. Alloy Compd. 490 (2010) 690–694.

[31] D. Shan, Y.J. Qu, Song, Ionic doping effects on crystal structure and relaxation character in $Na_{0.5}Bi_{0.5}TiO_3$ ferroelectric ceramics, J. Mater. Res. 22 (2007) 730–734.

[32] M. Popescu, C. Ghizdeanu, Cation distribution in cobalt ferrite–aluminates, Phys. Status Solidi A 52 (1979) K169–K172.

[33] M. Cernea, P. Galizia, I. Ciuchi, G. Aldica, V. Mihalache, L. Diamandescu, C. Galassi, $CoFe_2O_4$ magnetic ceramic derived from gel and densified by spark plasma sintering, J. Alloy Compd. 656 (2016) 854–862.

[34] L. Huitema, M. Cernea, A. Crunteanu, L. Trupina, L. Nedelcu, M.G. Banciu, A. Ghalem, M. Rammal, V. Madrangeas, D. Passerieux et al., Microwave dielectric properties of BNT–$BT_{0.08}$ thin films prepared by sol–gel technique, J. Appl. Phys. 119 (2016) 144103 (1–7).

[35] C.E. Ciomaga, C.S. Olariu, L. Padurariu, A.V. Sandu, C. Galassi, L. Mitoseriu, Low field permittivity of ferroelectric–ferrite ceramic composites: Experiment and modeling, J. Appl. Phys. 112 (2012) 094103 (1–12).

[36] A. Sakanas, R. Grigalaitis, J. Banys, L. Curecheriu, L. Mitoseriu, V. Buscaglia, Microstructural influence on the broadband dielectric properties of $BaTiO_3$–$Ni_{0.5}Zn_{0.5}Fe_2O_4$ core–shell composites: Experiment and modeling, J. Appl. Phys. 118 (2015) 174106 (1–8).

[37] A. Rahman, M.A. Rafiq, S. Karim, K. Maaz, M. Siddique, M.M. Hasan, Semiconductor to metallic transition and polaron conduction in nanostructured cobalt ferrite, J. Phys. D: Appl. Phys. 44 (2011) 165404 (1–6).

[38] N. Sivakumar, A. Narayanasamy, C.N. Chinnasamy, B. Jeyadevan, Influence of thermal annealing on the dielectric properties and electrical relaxation behaviour in nanostructured $CoFe_2O_4$ ferrite, J. Phys.: Condens. Mater. 19 (2007) 386201 (1–11).

[39] F. Maglia, I.G. Tredici, U. Anselmi-Tamburini, Densification and properties of bulk nanocrystalline functional ceramics with grain size below 50 nm, J. Eur. Ceram. Soc. 33 (2013) 1045–1066.

[40] P.G. Radaelli, Orbital ordering in transition-metal spinels, New J. Phys. 7 (2005) 1-22.

[41] S. Kalinin, D. Bonnell, Imaging mechanism of piezoresponse force microscopy of ferroelectric surfaces, Phys. Rev. B 65 (2002) 125408 (1–11).

[42] J.W. Wang, Y.G. Zhao, C. Fan, X.F. Sun, S. Rizwan, S. Zhang, P.S. Li, Z. Lin, Y.J Yang, W. Yan, Ferroelectric domain-controlled magnetic anisotropy in $Co_{40}Fe_{40}B_{20}/YMnO_3$ multiferroic heterostructure, Appl. Phys. Lett. 102 (2013) 102906 (1–5).

[43] Y.T. Yang, J. Li, X.L. Peng, B. Hong, X.Q. Wang, H.L. Ge, Electrical modulation of magnetism in multiferroic heterostructures at room temperature, J. Mater. Sci. 52 (2017) 3330–3336.

[44] P. Galizia, M. Cernea, V. Mihalache, L. Diamandescu, G. Maizza, C. Galassi, Easy batch–scale production of cobalt ferrite nanopowders by two–step milling: Structural and magnetic characterization, Mater. Design 130 (2017) 327–354.

[45] M.V. Limaye, S.B. Singh, S.K. Date, D. Kothari, R.V. Raghavendra, A. Gupta, V. Sathe, C.R. Jane, S.K. Kulkarni, High coercivity of oleic acid capped $CoFe_2O_4$ nanoparticles at room temperature, J. Phys. Chem. B 113 (2009) 9070–9076.

[46] P. Galizia, C.E. Ciomaga, L. Mitoseriu, C. Galassi, PZT–cobalt ferrite particulate composites: Densification and lead loss controlled by quite–fast sintering, J. Eur. Ceram. Soc. 37 (2017) 161–168.

[47] P. Galizia, C. Baldisserri, C. Capiani, C. Galassi, Multiple parallel twinning overgrowth in nanostructured dense cobalt ferrite, Mater. Design 109 (2016) 19–26.

[48] N.H. Tuan, L.H. Bac, L.V. Cuong, D.V. Thiet, T.V. Tam, D.D. Dung, Structural, Optical, and Magnetic Properties of Lead–Free Ferroelectric $Bi_{0.5}K_{0.5}TiO_3$ Solid Solution with $BiFeO_3$ Materials, J. Electron. Mater. 46 (2017) 3472–3478.

[49] Y. Zhang, J. Hu, F. Gao, H. Liu, H. Qin, Ab initio calculation for vacancy–induced magnetism in ferroelectric $Na_{0.5}Bi_{0.5}TiO_3$, Comput. Theor. Chem. 967 (2011) 284–288.

[50] T.L. Phan, P. Zhang, D.S. Yang, T.D. Thanh, D.A. Tuan, S.C. Yu, Origin of ferromagnetism in $BaTiO_3$ nanoparticles prepared by mechanical milling, J. Appl. Phys.113, 17E305 (2013) 1–3.

[51] A. Sundaresan, R. Bhargavi, N. Rangarajan, U. Siddesh, C.N.R. Rao, Ferromagnetism as a universal feature of nanoparticles of the otherwise nonmagnetic oxides, Phys. Rev. B74 (2006) 161306 (1–4).

[52] F. Tolea, M. N. Grecu, V. Kuncser, S. G. Constantinescu, D. Ghica, On the role of Fe ions on magnetic properties of doped TiO_2 nanoparticles, Appl. Phys. Lett. 106 (2015) 142404 (1–5).

[53] K. Maaz, A. Mumtaz, S.K. Hasanain, A. Ceylan, Synthesis and magnetic properties of cobalt ferrite ($CoFe_2O_4$) nanoparticles prepared by wet chemical route, J. Magn. Magn. Mater. 308 (2007) 289-–295.

[54] P. Poddar, H. Srikanth, S.A. Morrison, E.E. Carpenter, Inter–Particle Interactions and Magnetism in Manganese–Zinc Ferrite Nanoparticles, J. Magn. Magn. Mater. 288 (2005) 443–451.

Figure Captions

Fig.1. XRD patterns (CuK_α radiation) of (a) core–shell composite BNT–$BT_{0.08}/CoFe_2O_4$ powder, calcined at 700 °C, 2h in air and (b) sintered ceramic at 1100 °C, 10 min in air.

Fig.2. SEM image of core BNT–$BT_{0.08}$ powder calcined at 650 °C, 4 h in air (a) and SEM image of BNT–$BT_{0.08}/CoFe_2O_4$ core–shell powder dried at 100 °C (b).

Fig. 3. (a) BF–TEM and (b) detail images of the core-shell BNT–$BT_{0.08}/CoFe_2O_4$ calcined powder at 700 °C for 2h, in air. (c)-(e) HR–TEM of Area 1, Area 2 and between the two Areas (phases), respectively. (f) Corresponding SAED pattern of the calcined powder.

Fig. 4. (a) SEM micrograph of fracture surface of sintered ceramic BNT–$BT_{0.08}/CoFe_2O_4$ at 1100 °C, 10 min in air and, (b–d) corresponding chemical compositional mapping.

Fig.5. Frequency dependence of (a) real part of the permittivity, (b) loss tangent, and (c) of the AC conductivity for BNT–$BT_{0.08}/CoFe_2O_4$ sintered composite core-shell.

Fig.6. (a) Real (M′) and (b) imaginary (M′′) parts of electric modulus as a function of frequency, (c) Nyquist plot obtained at room temperature for BNT–$BT_{0.08}/CoFe_2O_4$ sintered composite core–shell.

Fig.7. Polarization hysteresis loop obtained by PUND method at room temperature for BNT–$BT_{0.08}/CoFe_2O_4$ sintered ceramic sample.

Fig. 8. Piezoelectric characterization and polarization hysteresis measurements of the BNT–$BT_{0.08}/CoFe_2O_4$ core–shell sintered ceramic. AFM contact mode topography (a); simultaneously acquired maps of amplitude (b) and phase (c) of piezoresponse.

Fig.9. Magnetic hysteresis curves recorded at 5 K (a) and 295 K (inset of (b)) for the core/shell hetero–nanostructure BNT–$BT_{0.08}/CoFe_2O_4$ powder; (b) shows the magnified part of the hysteresis loop in the low–field range, of the composite.

Table Captions

Table 1. Magnetic parameters of the core–shell BNT–$BT_{0.08}$/$CoFe_2O_4$ powder measured at 5 K and 295 K (results from the literature are reported as well, for comparison).